Electronic Supplementary Information (ESI)

Redefining the Roles of Alkali Activators for Porous Carbon

Yonghui Zhang,[†a,b] Xin Xu,[†a] Qingxuan Geng,[†c] Qingwei Li,[*c] Xiuli Li,[a] Yixuan Wang,[a] Zihuan Tang,[a] Biao Gao,[a] Xuming Zhang,[a] Paul K. Chu,[d] and Kaifu Huo [*a,b]

[a] The State Key Laboratory of Refractories and Metallurgy, Institute of Advanced Materials and Nanotechnology, Wuhan University of Science and Technology, Wuhan 430081, China

[b] Wuhan National Laboratory for Optoelectronics (WNLO), School of Optical and Electronic Information, Huazhong University of Science and Technology Wuhan 430074, China

[c] State Key Laboratory of Biobased Material and Green Papermaking, Advanced Research Institute for Multidisciplinary Science, Qilu University of Technology (Shandong Academy of Sciences), Daxue Road 3501, Jinan 250307, Shandong Province, China

[d] Department of Physics, Department of Materials Science and Engineering, and Department of Biomedical Engineering, City University of Hong Kong, Tat Chee Avenue, Hong Kong, Kowloon 999077, China

* Corresponding authors. liqingwei@qlu.edu.cn (Q. Li), kfhuo@hust.edu.cn (K. Huo).

† These authors contributed equally to this work.

Device Assembly and Electrochemical Measurements

The device was assembled of CK_1K_2-122 as electrodes and cellulose membrane with a diameter of 16 mm as a diaphragm in 6M KOH and $EMIMBF_4$. The preparation of the electrode method is similar to the three-electrode tests. The difference is that the slurry was coated on a circle with a diameter of 12 mm and the PTFE was replaced by PVDF in NMP. The mass of CK_1K_2-122 was calculated to be 8 mg according to the formula (1).

$$m_+/m_-=(C_-\times\Delta V_-)/(C_+\times\Delta V_+) \quad (1)$$

$$C=(I\times\Delta t)/(m\times\Delta V) \quad (2)$$

$$E=CV^2/(2\times3.6) \quad (3)$$

$$P=(3600\times E)/\Delta t \quad (4)$$

The $\Delta V(V)$, m (g) and C(F g^{-1}) represent the respective potential window, quality of active material and specific capacity of positive and negative electrode materials in the testing process of a three-electrode system, respectively. According to formula (2), the specific capacity (C, F g^{-1}) can be calculated. I (A) is the charge and discharge current. The Δt (s) is the time of discharge. The energy density (E, Wh kg^{-1}) and power density (P, W kg^{-1}) was calculated based on formula (3) and (4).

The b-value is one of the important parameters to measure the proportion of diffusion control and capacity control. This relationship can be determined by Equation 5.

$$i = av^b \quad (5)$$

The a and b are constants. The b value can be calculated by the linear relationship between log(i) and log(v).

The proportion of capacity-controlled and diffusion-controlled processes in the specific

capacity for different sweep speeds can be found by Equation (6).

$$i(v) = k_1 v + k_2 v^{1/2} \qquad (6)$$

$$i(v)/v^{1/2} = k_1 v^{1/2} + k_2 \qquad (7)$$

where i, v, k_1, and k_2 measure current, sweep speed, and constant, respectively. The values of k_1 (slope) and k_2 (intercept) can be calculated separately directly from a linear relationship. The formula can be deformed as Equation (7).

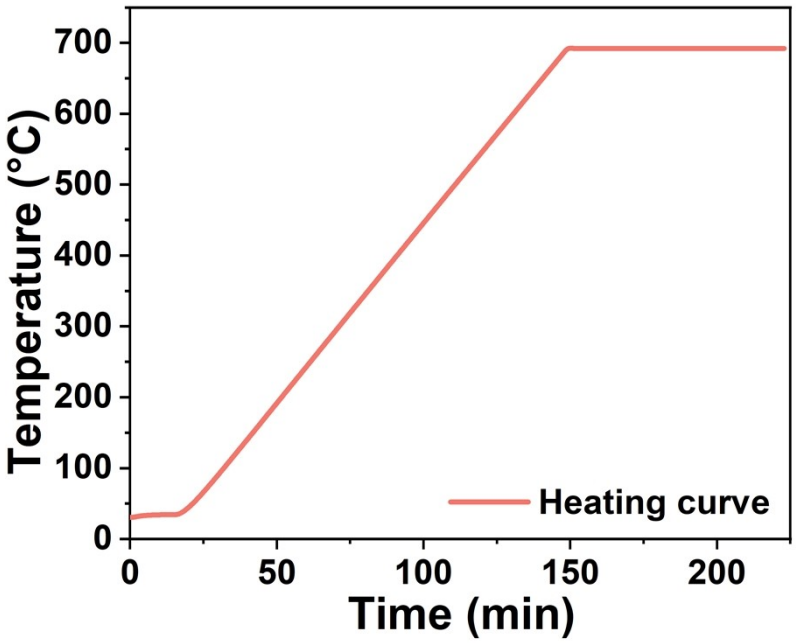

Figure S1. Temperature rise curve of TG.

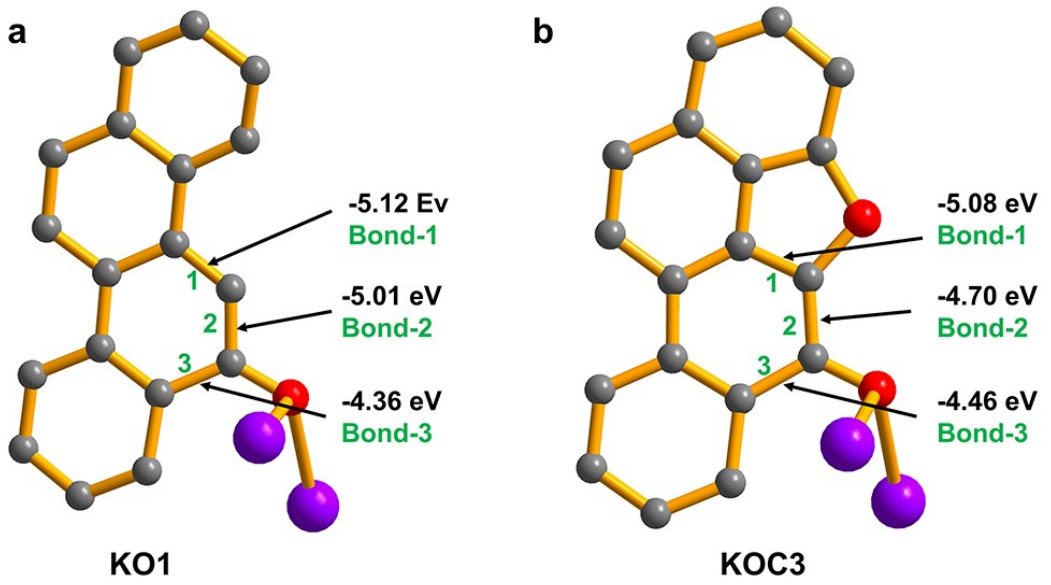

Figure S2. Bond energy schematic illustration of (a) KO1 model and (b) KOC3 model.

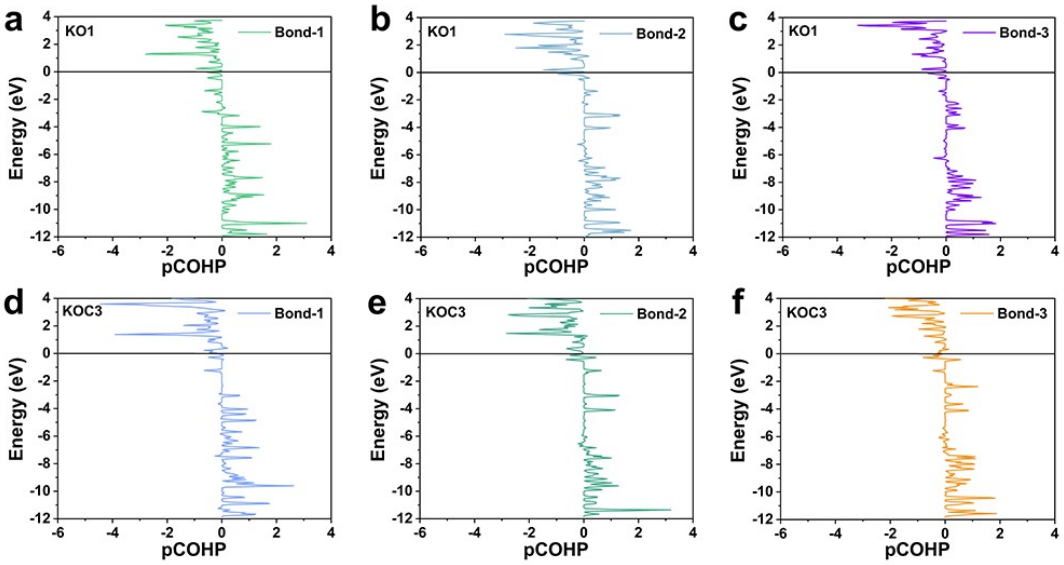

Figure S3. (a-c) Bond energy for KO1 model. (d-f) Bond energy for KOC3 model.

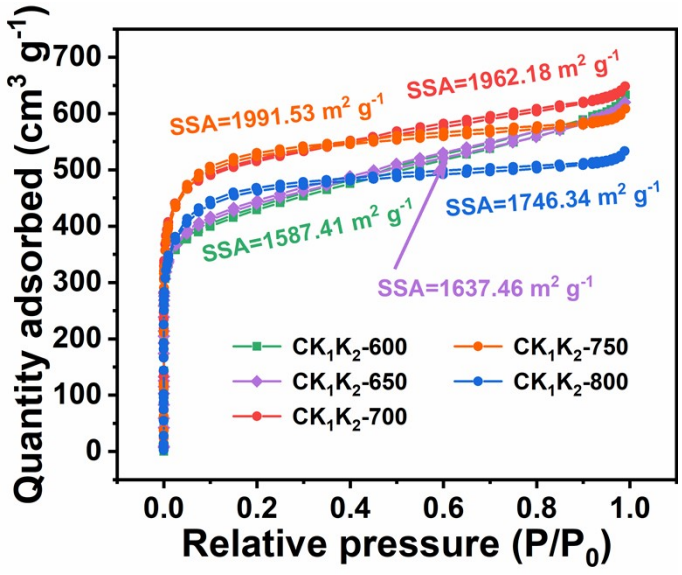

Figure S4 N_2 adsorption-desorption isotherms of CK_1K_2-TX (X=600, 650, 700, 750, 800).

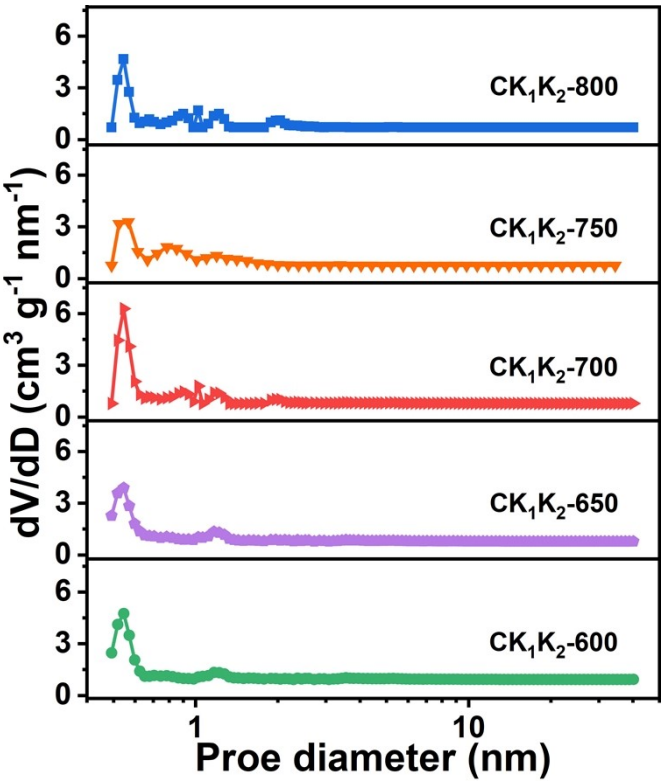

Figure S5 Pore size distribution of CK_1K_2-TX (X=600, 650, 700, 750, 800).

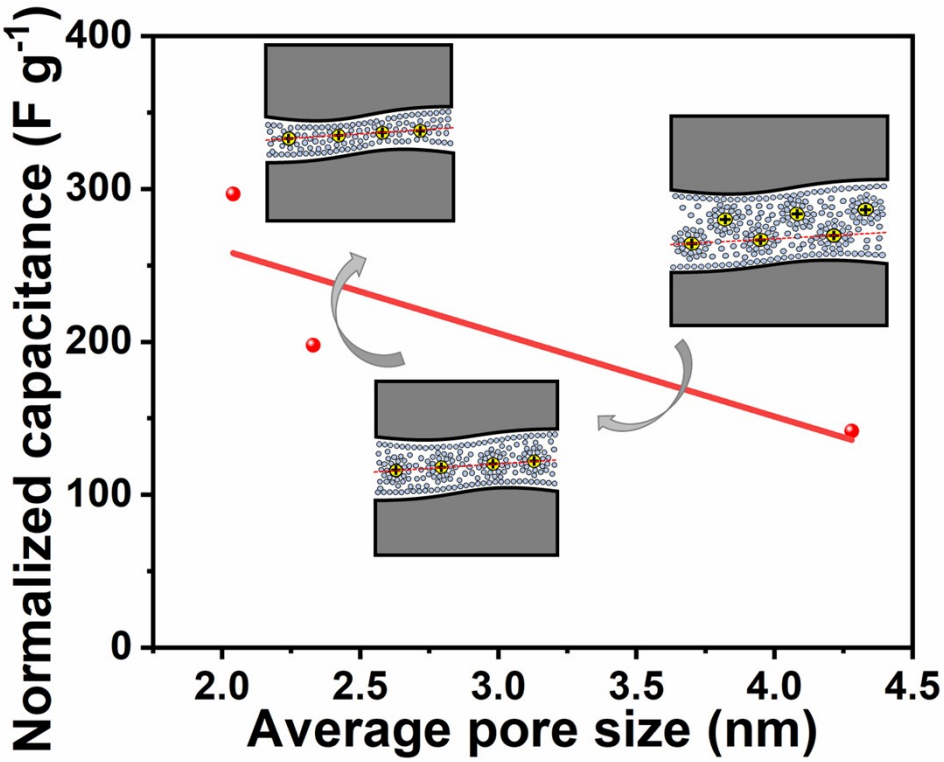

Figure S6. Plot of aperture size versus normalised capacitance (charge storage versus pore size correlation).

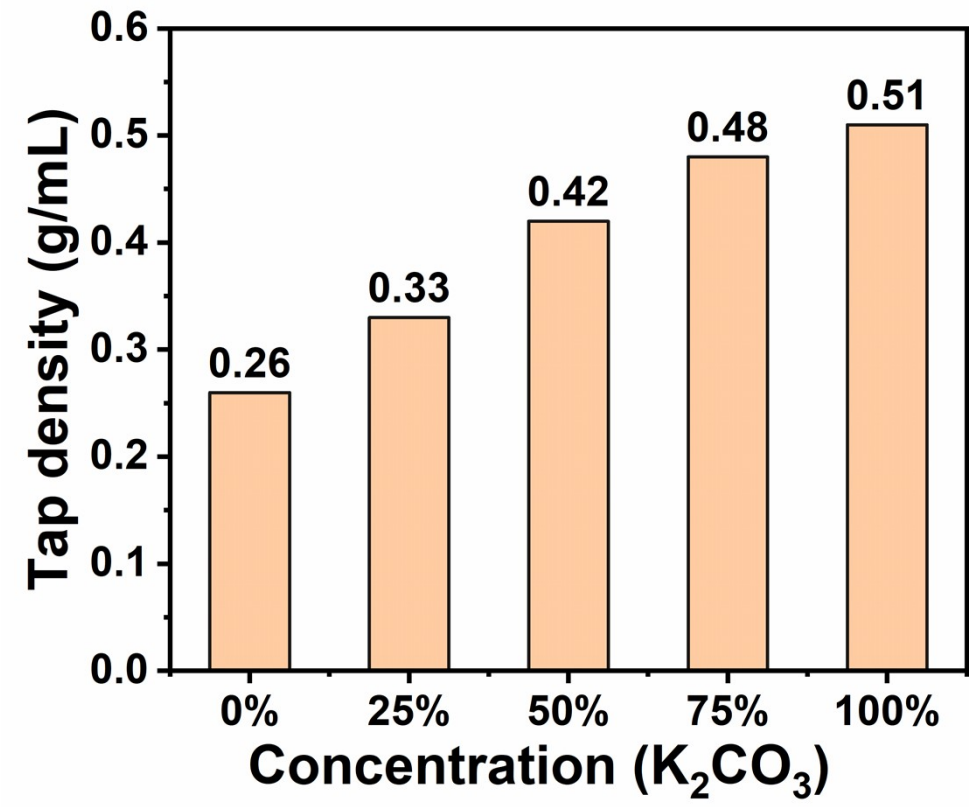

Figure S7. Tap density of different concentration.

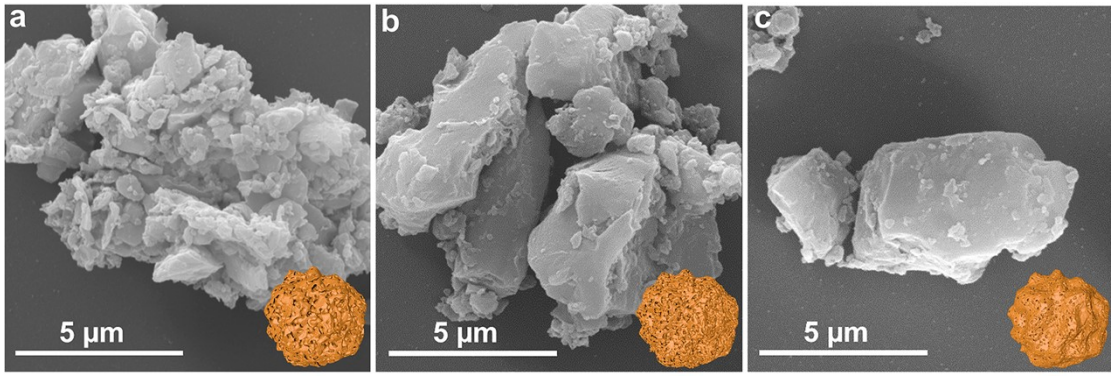

Figure S8. SEM images of (a) CK_1K_2-140, (b) CK_1K_2-122, and (c) CK_1K_2-104.

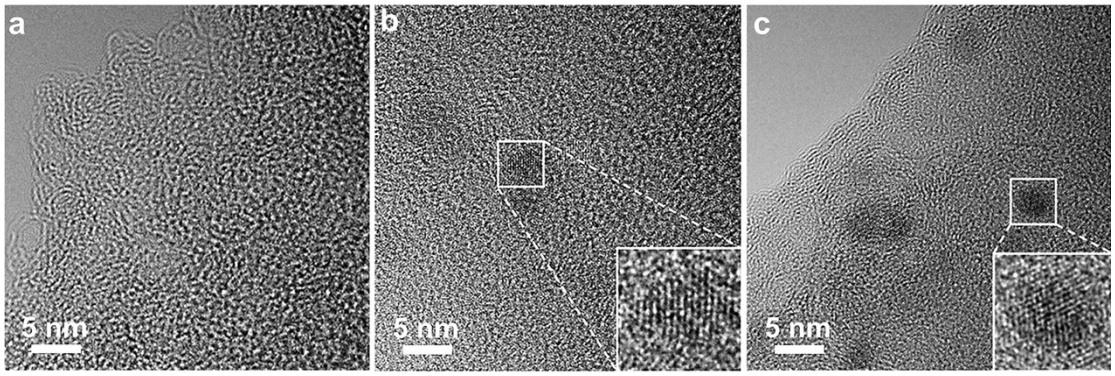

Figure S9.HRTEM images of (a) CK_1K_2-140, (b) CK_1K_2-122, and (c) CK_1K_2-104.

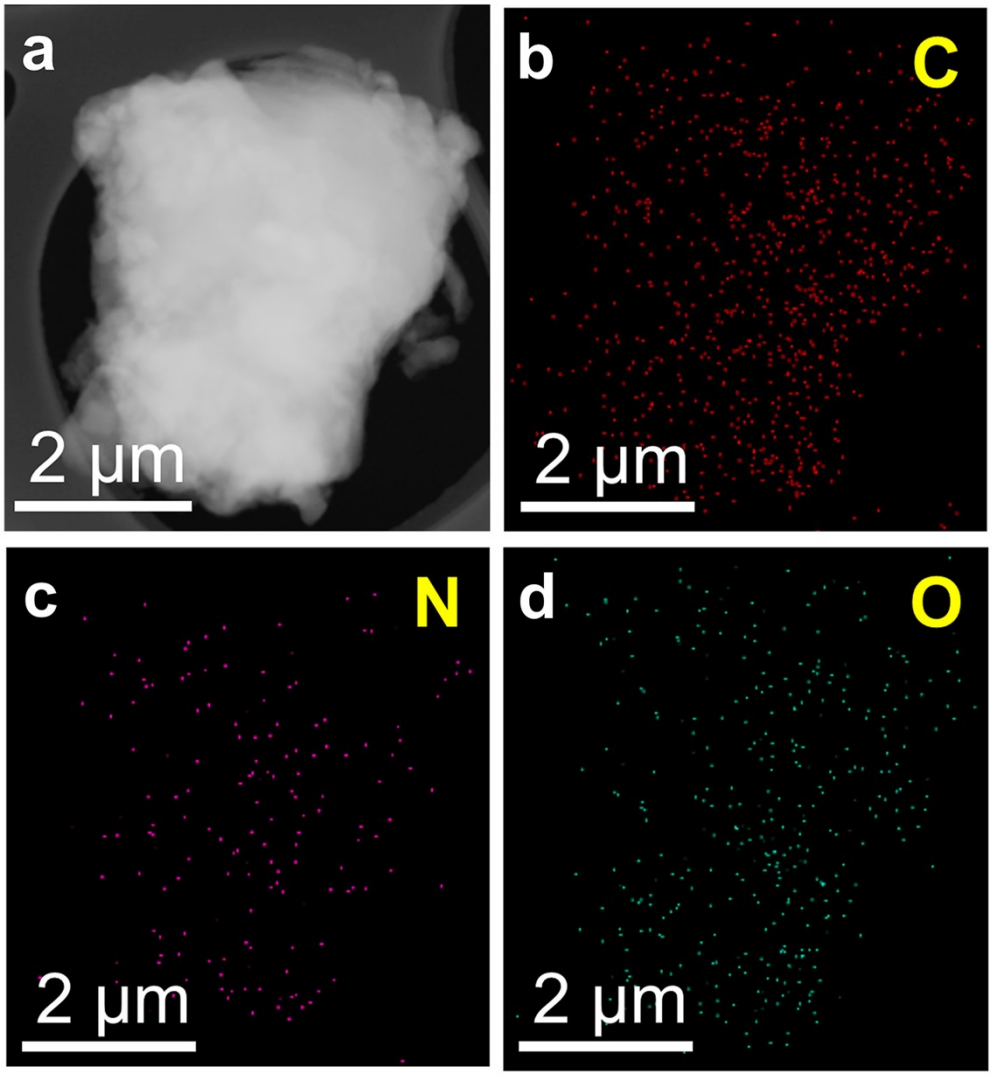

Figure S10. Elemental mapping of CK_1K_2-122.

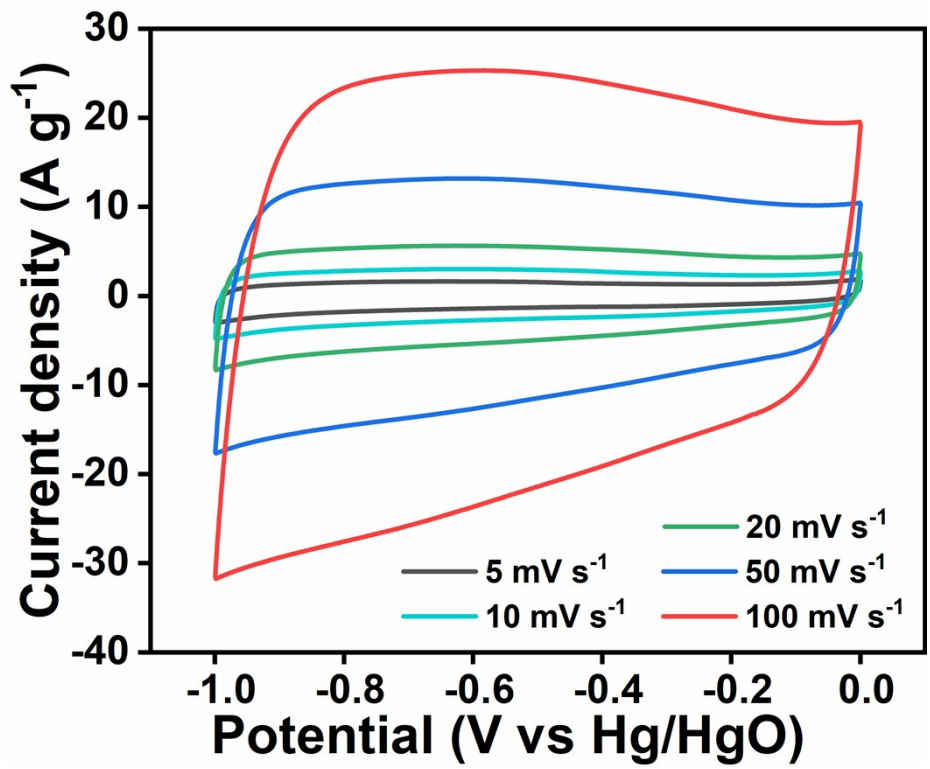

Figure S11. CV at 5-100 mV s^{-1} of CK_1K_2-122.

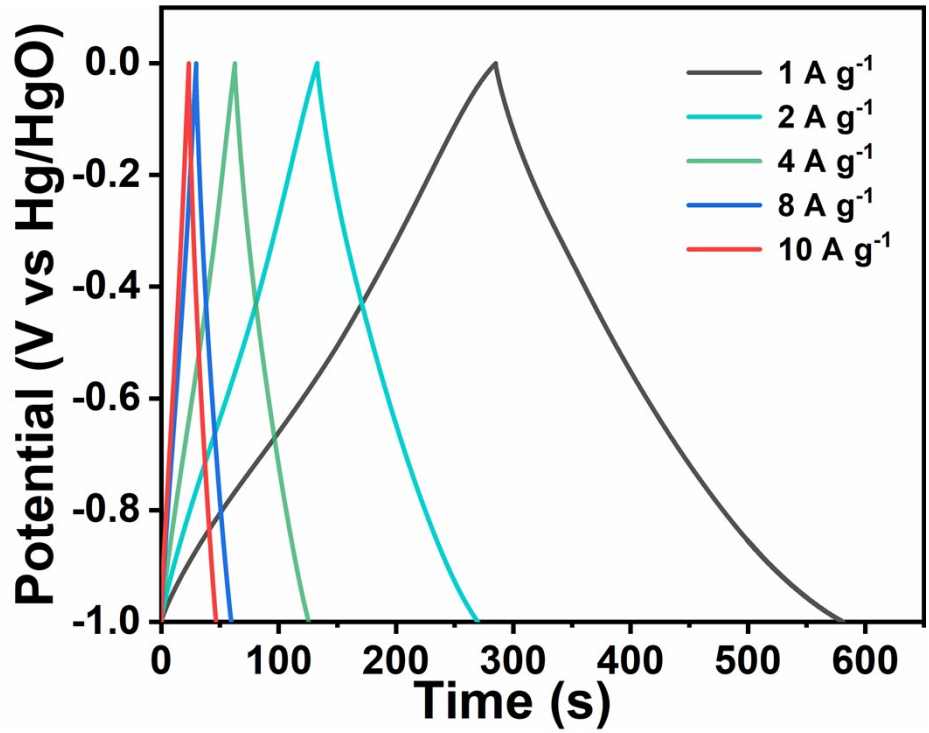

Figure S12. GCD curves at 1-10 A $g^{-1}$of CK_1K_2-122.

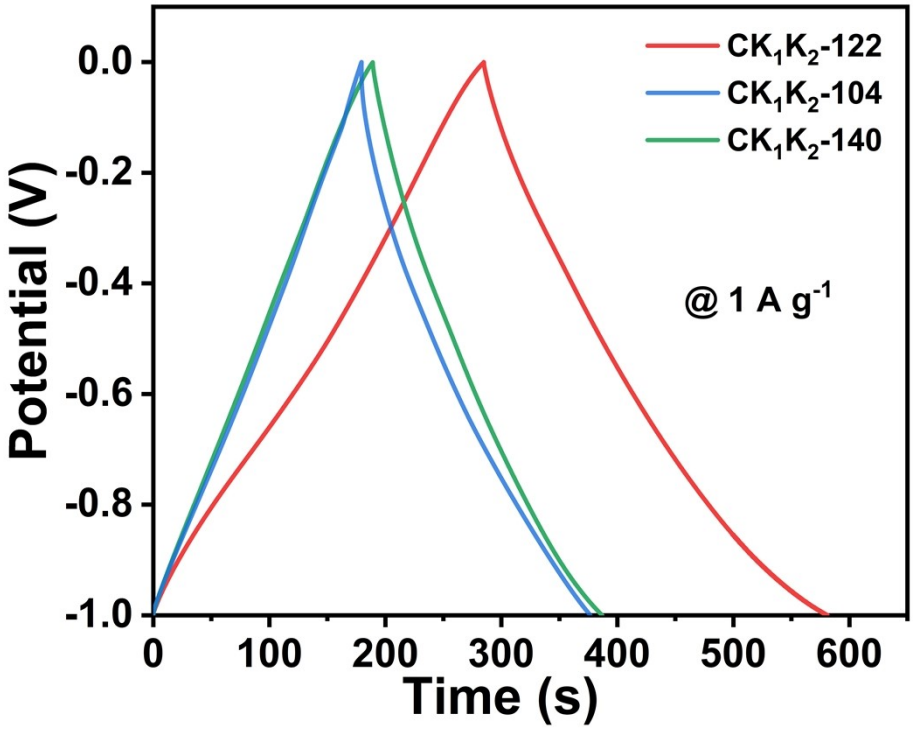

Figure S13. GCD curves of CK_1K_2-122, CK_1K_2-104, and CK_1K_2-140.

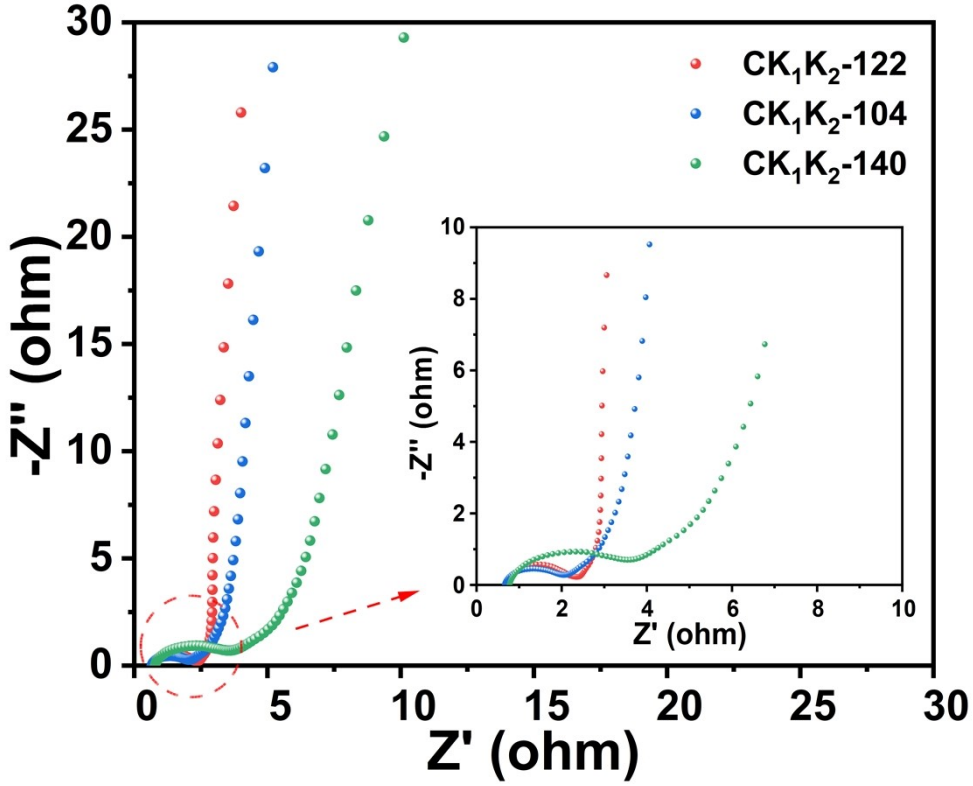

Figure S14. Electrochemical impedance spectroscopy (EIS) of CK_1K_2-1x(4-x) (x=0, 2, 4).

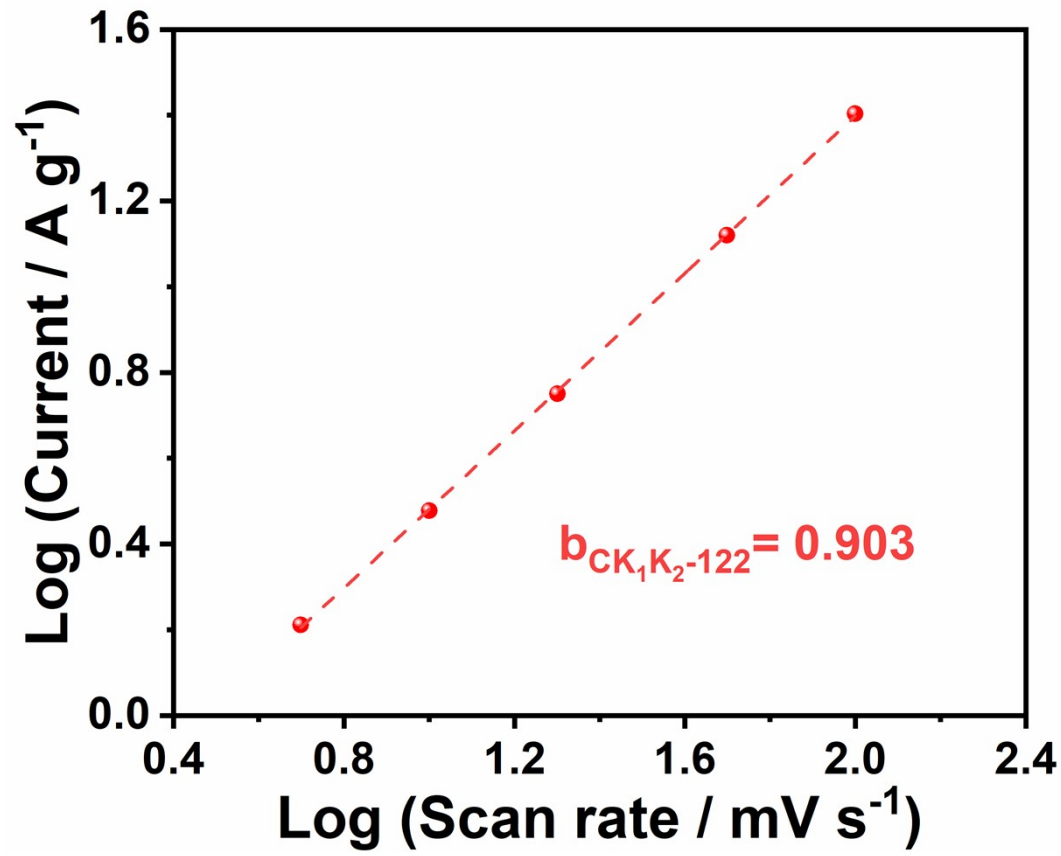

Figure S15. Logarithm relationship between scan rate and anodic peak current.

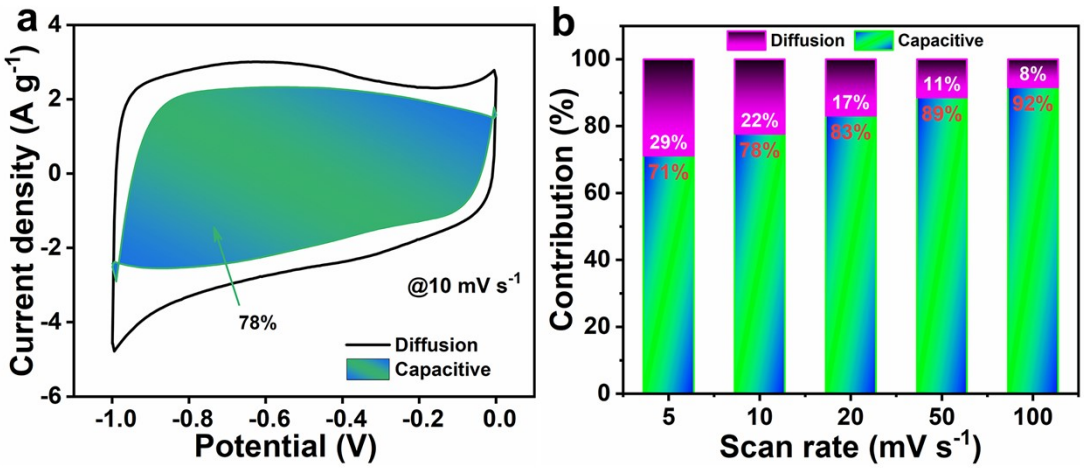

Figure S16. (a) Diffusion contribution and capacitive contribution at 10 mV s^{-1} and (b) the contribution proportions of at different scan rates of CK_1K_2-122.

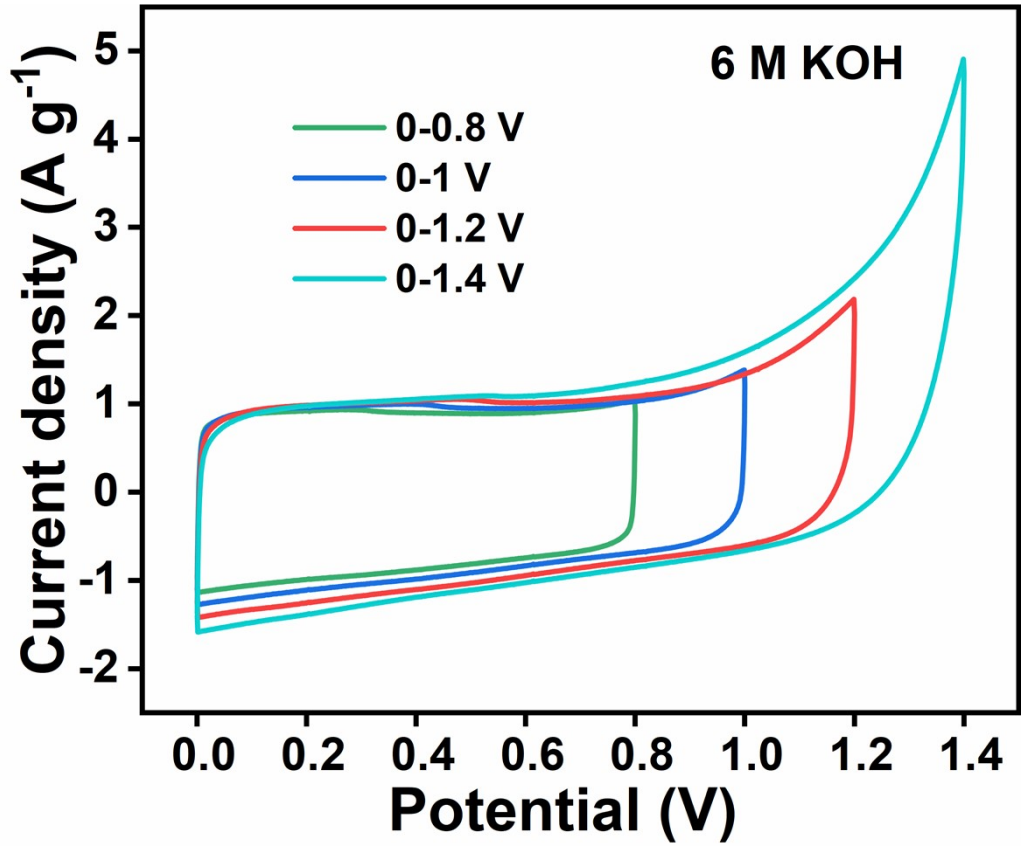

Figure S17. The CV curves of supercapacitor using 6 M KOH as electrolyte at different potential windows.

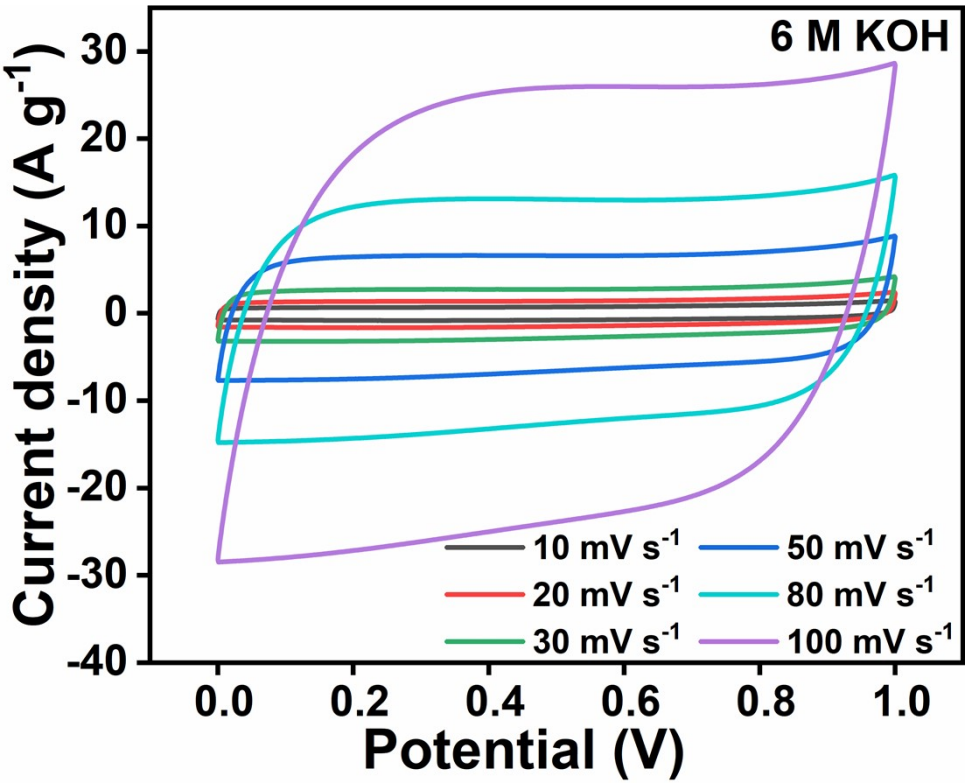

Figure S18. CV curves at 10-100 mV s^{-1}.

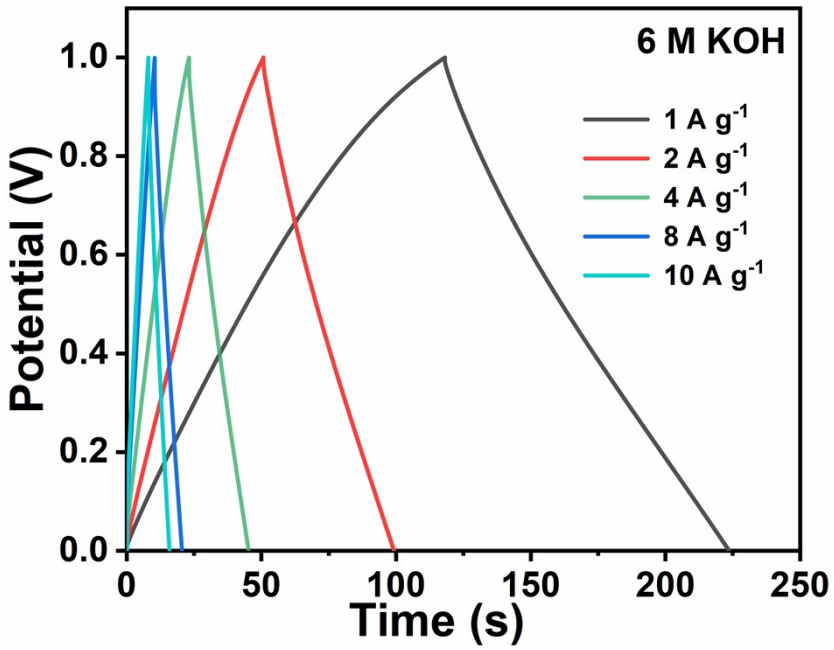

Figure S19. GCD at different current density from 1-10 A g^{-1}.

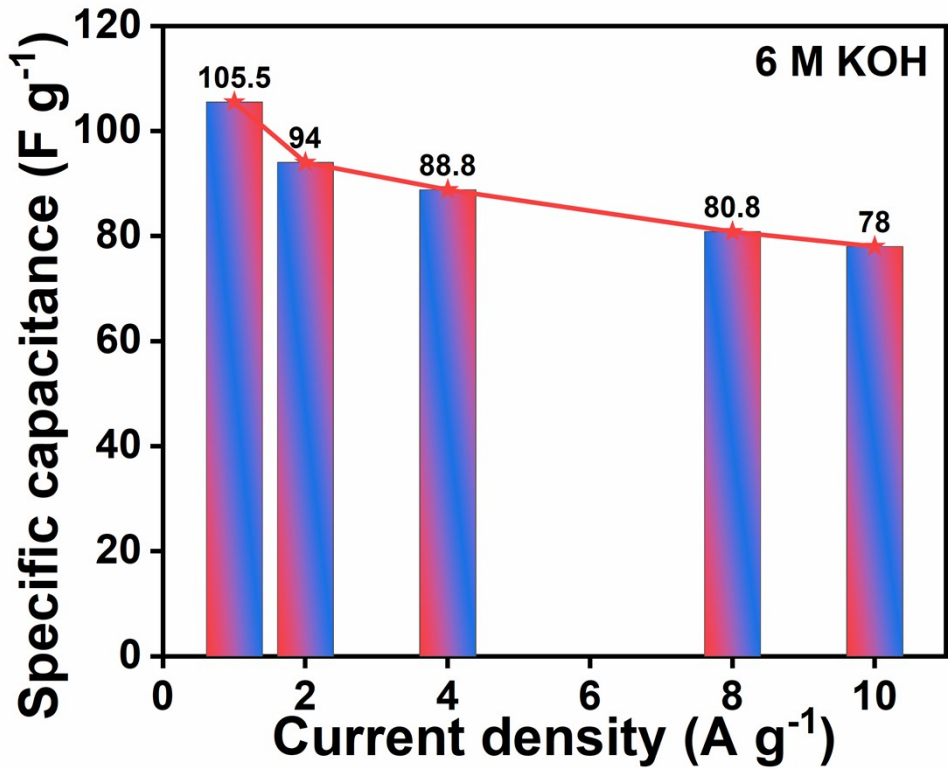

Figure S20. The specific capacitance of supercapacitor using 6 M KOH as electrolyte.

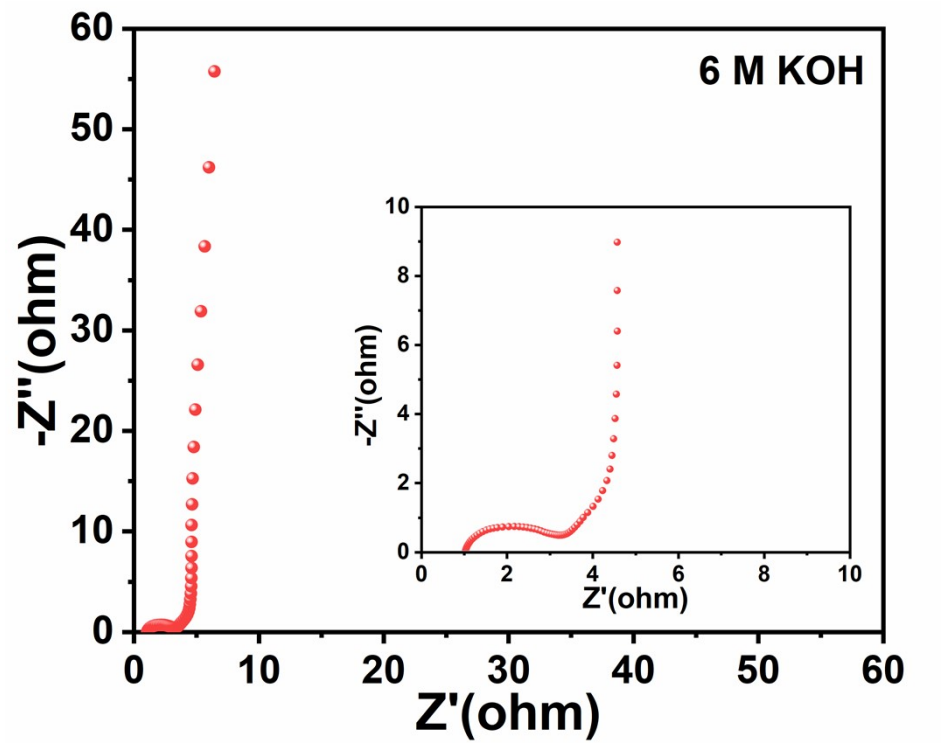

Figure S21. The EIS curves of supercapacitor using 6 M KOH as electrolyte.

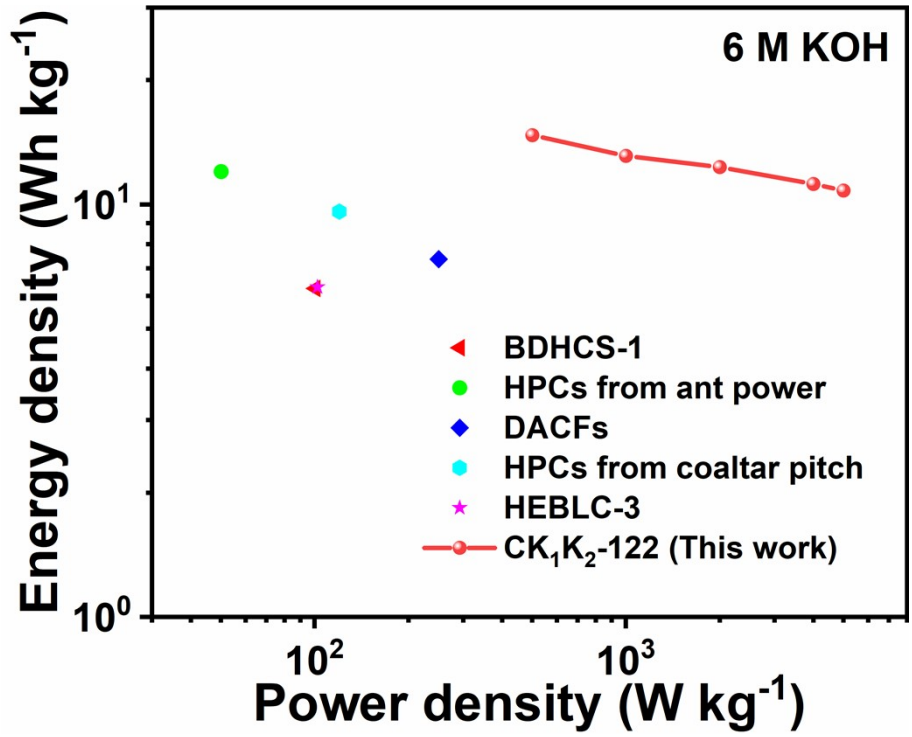

Figure S22. The Ragone plots of supercapacitor using 6 M KOH as electrolyte.

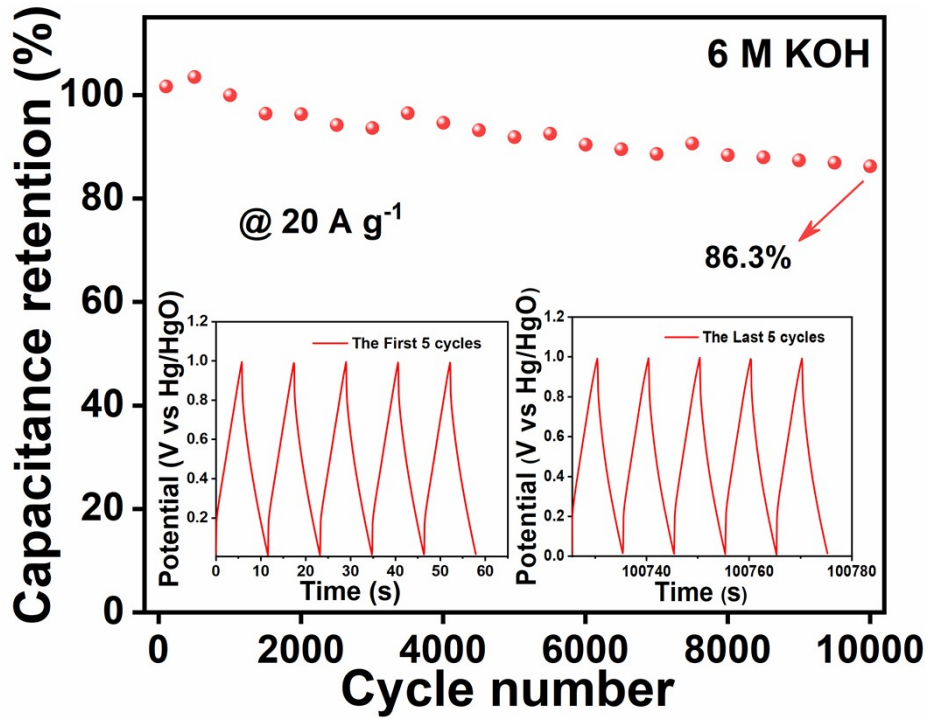

Figure S23. Cycling stability of supercapacitor using 6 M KOH as electrolyte at 20 A g^{-1}.

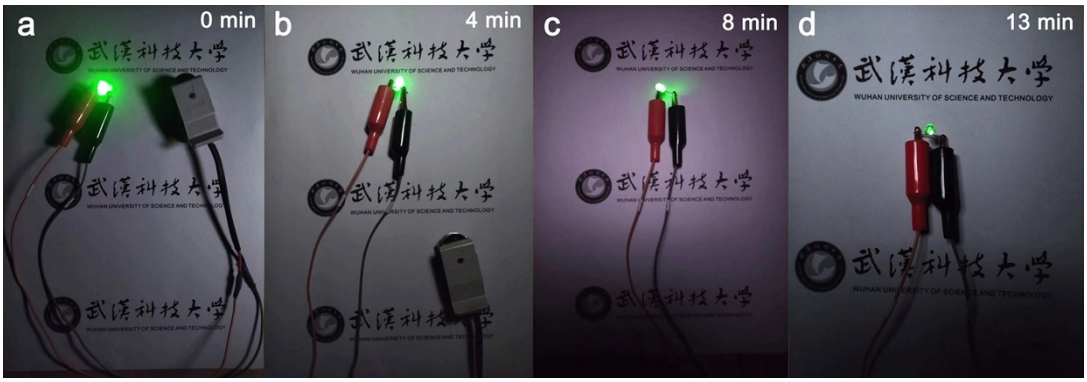

Figure S24. The LED light was powered by $EMIMBF_4$ and operated for 13 min, (a) 0 min, (b) 4 min, (c) 8 min, (d) 13 min.

Table S1. Specific surface area and pore size structure parameters of petroleum coke samples at 700 °C with different activator ratios.

Sample	S_{BET} (m^2 g^{-1})	S_{Mic} (m^2 g^{-1})	S_{Mic}/S_{BET} (%)	V_t (cm^3 g^{-1})	D_{av}(nm)
CK_1K_2-104	600.56	224.35	37.36	0.71	4.28
CK_1K_2-113	880.33	360.82	40.97	0.85	3.22
CK_1K_2-122	1962.18	1620.99	82.61	1.01	2.04
CK_1K_2-131	1928.45	1449.97	75.19	1.15	2.39
CK_1K_2-140	3373.79	2301.02	68.20	1.96	2.33

Table S2 Specific surface area and pore size structure parameters of CK_1K_2-TX with the same activator ratio of C : KOH : K_2CO_3=1 : 2 : 2 at different activation temperatures.

Sample	S_{BET} (m^2 g^{-1})	S_{Mic} (m^2 g^{-1})	S_{Mic}/S_{BET} (%)	V_t (cm^3 g^{-1})	D_{av}(nm)
CK_1K_2-600	1587.40	1105.82	69.67	0.98	2.47
CK_1K_2-650	1637.46	1185.34	72.39	0.96	2.35
CK_1K_2-700	1962.18	1620.99	82.61	1.01	2.04
CK_1K_2-750	1991.53	1768.02	88.78	0.94	1.89
CK_1K_2-800	1746.34	1561.31	89.40	0.83	1.89

Table S3. Different impedance values of CK_1K_2-1x(4-x) (x=0, 2, 4) obtained by Zview analysis.

Samples	R_{ct} (Ω)	R_s (Ω)
CK_1K_2-104	1.2	0.66
CK_1K_2-122	1.4	0.74
CK_1K_2-140	3.3	0.78

Table S4. Different impedance values of supercapacitor utilizing $EMIMBF_4$ and as electrolyte obtained by Zview analysis.

Electrolyte	R_{ct} (Ω)	R_s (Ω)
$EMIMBF_4$	15.5	3.69
KOH	1.6	1.04

Table S5. Electrochemical performance data of different carbon materials device compared with other device.

Carbon materials	Electrolyte	Voltage (V)	*E* (Wh kg^{-1})	*P* (W kg^{-1})	References
CK_1K_2-122	$BMIMBF_4$	0-3.5	114.4	1749	This work
HPCs	$BMIMBF_4$	0-3.6	107	900.0	[1]
N, S-C	PBI-H_3PO_4	0-1.0	9.75	50.00	[2]
HPNC-NS	$BMIMBF_4$	0-3.5	102	875	[3]
3DPAC	6 M KOH	0-2.75	79.4	5100	[4]
CL-700	6 M KOH	0-1.0	7.10	124.9	[5]
HCF800	6 M KOH	0-1.2	12.99	12.00 K	[6]
GHC-17	6 M KOH	0-1.0	14.65	27.30 K	[7]
PCCS	6 M KOH	0-1.0	9.00	227.0	[8]
NSHPC	6 M KOH	0-1.4	12.40	400.0	[9]
NP-HPC_4	1 M Na_2SO_4	0-1.6	21	50	[10]
N-S-HPC	1 M Na_2SO_4	0-1.8	19.89	450	[11]
NSUC-0.4	6 M KOH	0-1.0	7.4	100	[12]
S, N-PIC-1	$BMIMBF_4$	0-3.0	40.95	749.24	[13]

Reference

1. G. Y. Zhao, C. Chen, D. F. Yu, L. Sun, C. H. Yang, H. Zhang, Y. Sun, F. Besenbacher and M. Yu, *Nano Energy,* 2018, **47**, 547−555.
2. L. Chen, C. Lian, H. Jiang, L. Chen, J. Yan, H. Liu and C. Li, *Chem. Eng. Sci.,* 2020, **217**, 115496.
3. J. H. Hou, C. B. Cao, F. Idrees and X. L. Ma, *ACS Nano,* 2015, **9**, 2556−2564.
4. X. B. Liu, C. G. Lai, Z. C. Xiao, S. Zou, K. X. Liu, Y. H. Yin, T. X. Liang and Z. P. Wu, *ACS Appl. Energy Mater.,* 2019, **2**, 3185−3193.
5. Z. L. Liu, D. Tian, F. Shen, P. C. Nnanna, J. G. Hu, Y. M. Zeng, G. Yang, J. S. He and S. H. Deng, *J. Power Sources*, 2020, **458**, 228057.
6. Y. W. Liu, Q. Liu, L. Wang, X. F. Yang, W. Y. Yang, J. J. Zheng and H. L. Hou, *ACS Appl. Mater. Interfaces,* 2020, **12**, 4777−4786.
7. Q. Zhang, K. Han, S. Li, Li, J. Li and K. Ren, *Nanoscale,* 2018, **10**, 2427−2437.
8. H. Y. Jia, J. W. Sun, X. Xie, K. B. Yin and L. T. Sun, *Carbon,* 2019, **143**, 309−317.
9. S. L. Huo, M. Q. Liu, L. L. Wu, M. J. Liu, M. Xu, W. Ni and Y. M. Yan, *J. Power Sources,* 2018, **387**, 81−90.
10. S. Y. Wang, J. D. Li, Y. H. Ke, Y. L. Wei and D. W. Wang, *Ionics,* 2022, **28**, 2377−2388.
11. K. Ning, G. Z. Zhao, H. X. Liu, M. Z. Hu, F. Huang, L. Zhang, G. Zhu, H. Y. Wang and J. Y. Shi, *Diamond and Related Materials,* 2022, **126**, 109080.
12. W. J. Lu, L. N. Hao and Y. W. Wang, *Micromachines,* 2022, **13**, 905.
13. S. Wu, X. T. Yan, X. Sun, S. Tian, J. J. Wang, C. Y. Liu, S. Q. Sun, L. Wu, X. F. Zhao and Q. L. Yang, *J. Energy Storage,* 2023, **71**, 108152.